Network Structured CuWO$_4$/BiVO$_4$/Co-Pi Nanocomposite for Solar Water Splitting

Ben Peng [1], Mengyang Xia [2], Chao Li [2], Changshen Yue [1] and Peng Diao [2,*]

[1] Central Research Institute of Building and Construction Co. LTD., Energy Convention and Environment Protection Co. LTD., State Key Laboratory of Iron & Steel industry Environmental Protection, Beijing 100088, China; pengben@cribc.com (B.P.); yuecs163@163.com (C.Y.)

[2] Key Laboratory of Aerospace Materials and Performance (Ministry of Education), School of Materials Science and Engineering, Beihang University, Beijing 100191, China; buaamyxia@126.com (M.X.); nwpuvip@yeah.net (C.L.)

* Correspondence: pdiao@buaa.edu.cn; Tel.: +86-10-8233-9562

Abstract: A network structured CuWO$_4$/BiVO$_4$ nanocomposite with a high specific surface area was prepared from CuWO$_4$ nanoflake (NF) arrays via a method that combined drop-casting and thermal annealing. The obtained CuWO$_4$/BiVO$_4$ exhibited high catalytic activity toward photoelectrochemical (PEC) water oxidation. When cobalt phosphate (Co-Pi) was coupled with CuWO$_4$/BiVO$_4$, the activity of the resulting CuWO$_4$/BiVO$_4$/Co-Pi composite for the oxygen evolution reaction (OER) was further improved. The photocurrent density (J_{ph}) for OER on CuWO$_4$/BiVO$_4$/Co-Pi is among the highest reported on a CuWO$_4$-based photoanode in a neutral solution. The high activity for the PEC OER was attributed to the high specific surface area of the composite, the formation of a CuWO$_4$/BiVO$_4$ heterojunction that accelerated electron–hole separation, and the coupling of the Co-Pi co-catalyst with CuWO$_4$/BiVO$_4$, which improved the charge transfer rate across composite/solution interface.

Keywords: photoelectrochemical water splitting; oxygen evolution reaction; copper tungstate; bismuth vanadate; cobalt phosphate

1. Introduction

Photoelectrochemical (PEC) water splitting is a promising way to capture solar energy and to store it in the chemical bonds of two products, H$_2$ and O$_2$ [1]. There are two half-cell reactions for PEC water splitting: a hydrogen evolution reaction (HER) and an oxygen evolution reaction (OER). Between them, the OER is the more sluggish reaction because it involves the removal of four electrons from two water molecules. In previous studies, N-type semiconductors, such as TiO$_2$ [2], ZnO [3,4], WO$_3$ [5–8], Fe$_2$O$_3$ [6,9], Ag$_3$PO$_4$ [10], BiVO$_4$ [11,12], and CuWO$_4$ [13,14], whose valence band edges are higher than the redox potential of the O$_2$/H$_2$O couple, have been employed as the photoanode materials for such PEC OER. CuWO$_4$ has been regarded as a promising photoanode material [13–20] due to its appropriate bandgap energy (2.3–2.4 eV), positive valence band edge potential (at ca. 2.8 V vs. reversible hydrogen electrode (RHE)) [13], low toxicity, and, most importantly, high stability in neutral and acid solutions. However, as compared with the highly active n-type semiconductors, the activity of CuWO$_4$ for PEC OER is still low because of its indirect bandgap and poor charge transport property [18], which results in the accumulation of photoinduced holes, thereby increasing the recombination. Therefore, increasing both the electron–hole separation rate and the charge transfer rate across the CuWO$_4$/solution interface are two possible ways of improving the activity of CuWO$_4$ for PEC OER.

Constructing a heterojunction by using two n-type semiconductors whose band edges match well with each other is an effective strategy to accelerate the electron–hole separation [6,21]. For example, it has been demonstrated that the composites of WO_3/Fe_2O_3 [6], $CuWO_4/CdS$ [19] $WO_3/CuWO_4$ [20], and $WO_3/BiVO_4$ [21,22] have exhibited enhanced activity toward PEC OER due to the formation of heterojunctions. $BiVO_4$ is an n-type semiconductor with a band gap of ca. 2.3 eV, which is quite similar to that of $CuWO_4$. The conduction and valence band edges of $BiVO_4$ are located at ca. 0 V and 2.3 V versus RHE, respectively, making $BiVO_4$ a good candidate to form a band-structure-matched heterojunction with other n-type semiconductors, such as WO_3, Fe_2O_3, and $CuWO_4$ [14,21–24]. The formation of $WO_3/BiVO_4$, $Fe_2O_3/BiVO_4$, and $CuWO_4/BiVO_4$ heterojunctions significantly promotes the electron–hole separation rate and benefits the improvement of the PEC OER efficiency. Coupling a semiconductor with an electrochemical OER co-catalyst is another way to enhance the activity of photoanode materials for water oxidation, because the cocatalyst can improve the charge transfer rate at the electrode/solution interface. Cobalt phosphate (Co-Pi) is an efficient cocatalyst that has been widely used to boost the performance of photoanode materials for PEC OER [3,5,6,11,12].

In this work, we prepared $CuWO_4/BiVO_4$-composite nanoflakes (NFs) via a drop-casting and thermal annealing method, with $CuWO_4$ NFs as templates. A layer of Co-Pi was deposited onto the surface of $CuWO_4/BiVO_4$ as a co-catalyst. We demonstrated that the obtained network-structured $CuWO_4/BiVO_4/Co-Pi$ nanocomposite exhibited a significantly improved activity for PEC OER. The high activity of the nanocomposite was ascribed to the high specific surface area, the electron–hole separation rate enhanced by the $CuWO_4/BiVO_4$ heterojunction, and the accelerated charge transfer rate at the semiconductor/solution interface due to the presence of Co-Pi.

2. Results and Discussion

The network-structured $CuWO_4/BiVO_4$-composite NFs were prepared from $CuWO_4$ NFs via a method that combined drop-casting and thermal annealing. The WO_3 NFs grown on the fluorine-doped tin oxide (FTO) substrate were used as sacrificial templates to synthesis $CuWO_4$ NFs via a thermal solid phase reaction [13]. The resulting $CuWO_4$ NFs were used to fabricate a $CuWO_4/BiVO_4$ composite, and the procedure is shown schematically in Scheme 1a. Briefly, Bi precursor solution was drop-cast on the surface of the FTO-supported $CuWO_4$ NFs, and the sample was annealed in air to obtain the $CuWO_4/BiVO_4$-composite NFs. Pure $BiVO_4$ films were also prepared using the same method, in which the mixed precursor solution was drop-cast on bare FTO substrates (Scheme 1b). The Co-Pi layer was deposited on the surface of $CuWO_4/BiVO_4$ using a photo-assisted electrodeposition method described elsewhere [6].
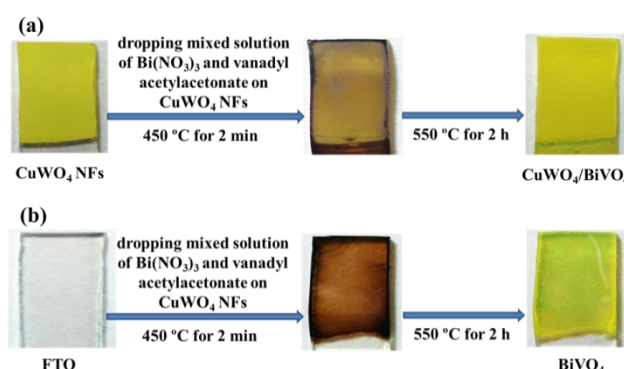
Scheme 1. Schematic representation of the preparation of (**a**) the $CuWO_4/BiVO_4$-composite NFs and (**b**) the pure $BiVO_4$ film on the fluorine-doped tin oxide (FTO) substrate via a method that involved drop-casting and thermal annealing.

Figure 1a–c show the typical scanning electron microscopic (SEM) images of the WO_3 NFs, $CuWO_4$ NFs, and the $CuWO_4/BiVO_4$-composite NFs, respectively. The WO_3 sample, synthesized by

hydrothermal growth, has a network structure, which was composed of the perpendicularly aligned WO_3 NFs (Figure 1a). These WO_3 NFs were used as sacrificial templates to synthesize $CuWO_4$, and $Cu(NO_3)_2$ solution was drop casted onto the surface of WO_3 NFs. During annealing, $Cu(NO_3)_2$ decomposed and produced CuO, which reacted with WO_3 to form $CuWO_4$. After annealing at 550 °C for 2 h, the WO_3 NFs were completely converted into $CuWO_4$ NFs [13]. As shown in Figure 1b, the obtained $CuWO_4$ retained the microstructure of the WO_3 NF templates. The size and thickness of the $CuWO_4$ NFs was ca. 0.5~2 μm and 20~50 nm, respectively. The NF structure of $CuWO_4$ provides a large specific surface area, which not only benefits the dispersion of the bismuth precursor ($Bi(NO_3)_3$) solution on the surface of $CuWO_4$, but also contributes to the formation of a large area $CuWO_4/BiVO_4$ heterojunction. Figure 1c clearly demonstrates that, after the drop-casting of the Bi ($NO_3)_3$ precursor solution and the follow-up thermal annealing at 550 °C for 2 h, the resulting $CuWO_4/BiVO_4$ composite still kept the NF network structure. The high-magnification SEM image (the inset of Figure 1c) shows that, compared with pure $CuWO_4$ NFs (see Figure 1b), the composite NFs became thicker and their surfaces became rougher, both suggesting the successful deposition of $BiVO_4$ onto the surface of the $CuWO_4$ NFs. In fact, the obtained $CuWO_4/BiVO_4$ nanocomposite can be regarded as a film that possesses a network structure composed of numerous intersected NFs.
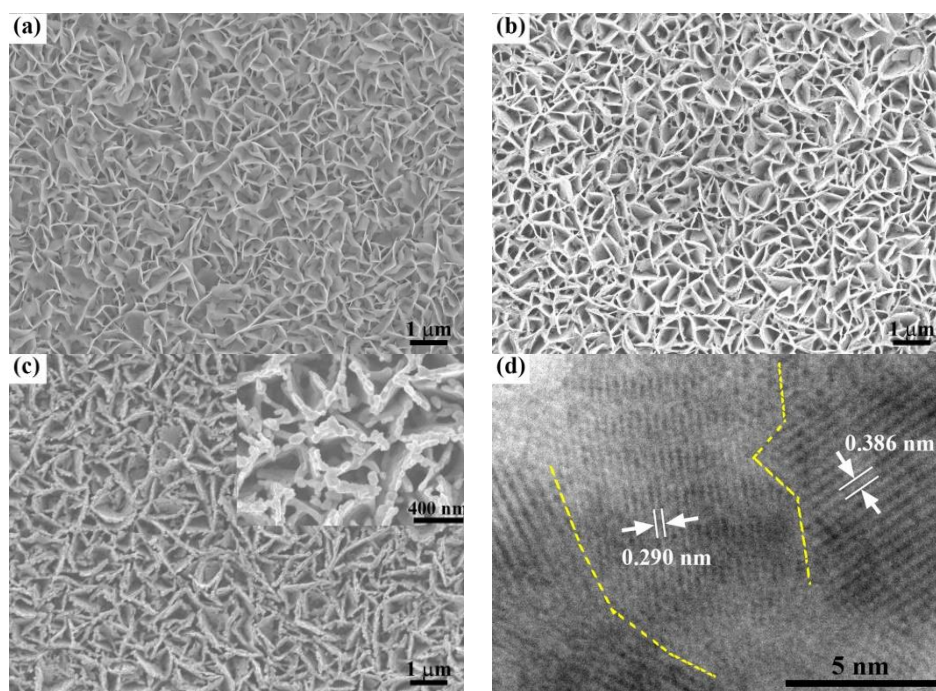
**Figure 1.** SEM images of the (**a**) WO_3 NFs; (**b**) $CuWO_4$ NFs, and (**c**) $CuWO_4/BiVO_4$-composite NFs; (**d**) high-resolution TEM image of the $CuWO_4/BiVO_4$-composite NFs.

High-resolution tunneling electron microscope (TEM) was employed to characterize the crystal structure of the composite NFs, and the result is presented in Figure 1d. The fringe with interplanar spacing of 0.290 nm and 0.386 nm can be clearly identified, which corresponded to the (040) plane of monoclinic $BiVO_4$ and the (110) lattice plane of triclinic $CuWO_4$, respectively. Moreover, the crystal boundaries between $CuWO_4$ and $BiVO_4$ can also be seen in Figure 1d, confirming the formation of a $CuWO_4/BiVO_4$ heterojunction. X-ray diffraction (XRD) was also used to characterize the crystal structure of the $CuWO_4/BiVO_4$-composite NFs, and the results are shown in Figure 2. The XRD spectrum of the composite NFs shows significantly enhanced diffraction intensity at 2θ of 19.0 and 28.9 degrees, where there happen to be the two most intense diffraction peaks (011) and (121) of monoclinic $BiVO_4$. This result provides strong evidence that the enhanced XRD intensity of the composite was

due to the diffraction contribution of $BiVO_4$. Therefore, we can conclude that the $CuWO_4/BiVO_4$ composite was successfully prepared by the drop-casting and thermal annealing method.
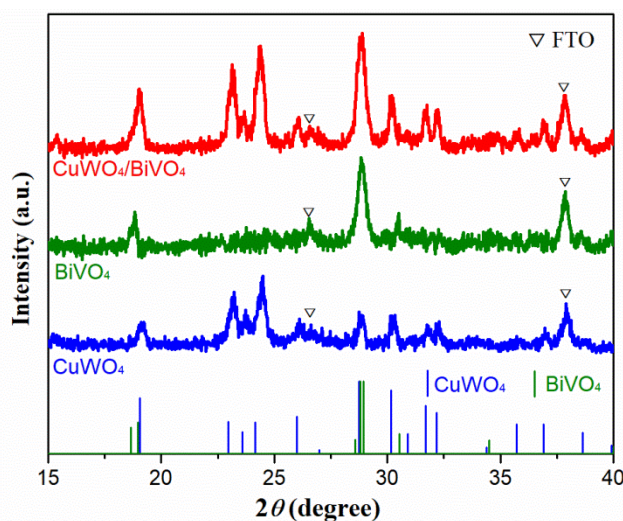
**Figure 2.** XRD patterns of $CuWO_4$, $BiVO_4$, and the $CuWO_4/BiVO_4$-composite NFs.

Light absorption is one of the crucial factors influencing the photo-to-chemical conversion efficiency of a photoelectrode material for water splitting. We measured the light absorption property of the $CuWO_4/BiVO_4$-composite NFs by using UV–Vis diffuse reflectance spectroscopy, and the results are shown in Figure 3a. The pure $CuWO_4$ and $BiVO_4$ films exhibited an onset absorption wavelength at ca. 525 nm and 530 nm, corresponding to the band edge absorption of $CuWO_4$ and $BiVO_4$, respectively. The band gap energies for $CuWO_4$ and $BiVO_4$, which were obtained from Tauc plots (see Figure 3b), were 2.37 eV and 2.36 eV, respectively. These values were in good agreement with those reported in literature [11–18] and are much smaller than that of WO_3 [6,25], ensuring that both $CuWO_4$ and $BiVO_4$ absorb more light than WO_3. The quite similar bandgap energy between $CuWO_4$ and $BiVO_4$ implies that the formation of the $CuWO_4/BiVO_4$ heterojunction cannot extend the light absorption range. This is also confirmed in UV–Vis absorption spectra of the $CuWO_4/BiVO_4$ composite. As shown in Figure 3a, after the formation of the $CuWO_4/BiVO_4$ heterojunction, the composite still showed an onset absorption wavelength of ca. 530 nm, which is the same as that of $BiVO_4$.
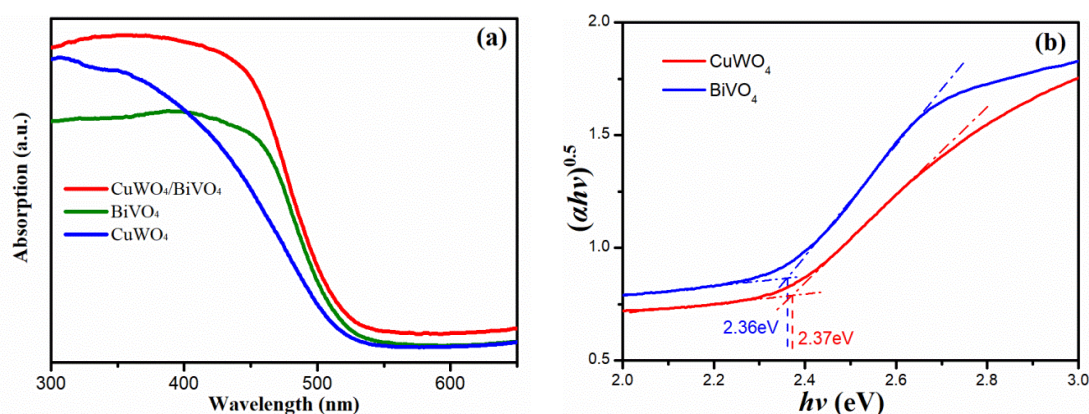
Figure 3. (**a**) UV–Vis absorption spectra of $CuWO_4$, $BiVO_4$, and the $CuWO_4/BiVO_4$ composite; (**b**) The corresponding Tauc plots of $CuWO_4$ and $BiVO_4$.

The PEC OER performances of the $CuWO_4$, $CuWO_4/BiVO_4$, and $CuWO_4/BiVO_4/Co$-Pi composites were evaluated using linear sweep voltammetry (LSV) in the dark and under 100 mW·cm^2 illumination. Figure 4a shows the LSV of the above photoanodes in a sodium phosphate buffer (pH

= 7) solution in the dark and under irradiation. Without illumination, no oxidation current could be observed on all the photoanodes within the entire potential sweep region, suggesting that they were all electrochemically inert for water oxidation in the dark. However, when illuminated, each photoanode showed an oxidation photocurrent density (J_{ph}), which had been proven to originate from the PEC OER [13–19]. The $CuWO_4/BiVO_4$ composite showed a much larger J_{ph} than the $CuWO_4$ NFs in the potential range from 0 V to 1.4 V versus RHE. As shown in Figure 4a, the OER onset potential of $CuWO_4/BiVO_4$ was 0.66 V versus RHE, which was negatively shifted ca. 0.1 V compared with $CuWO_4$. The J_{ph} value on $CuWO_4$ NFs at 1.23 V versus RHE is ca. 0.33 mA·cm^{-2}, which was in good agreement with the one reported previously [13]. However, after the formation of the $CuWO_4/BiVO_4$ heterojunction, J_{ph} on the composite at the same potential was increased to 0.67 mA·cm^{-2}, which was ca. 2 times higher than that on the $CuWO_4$ NF photoanode.
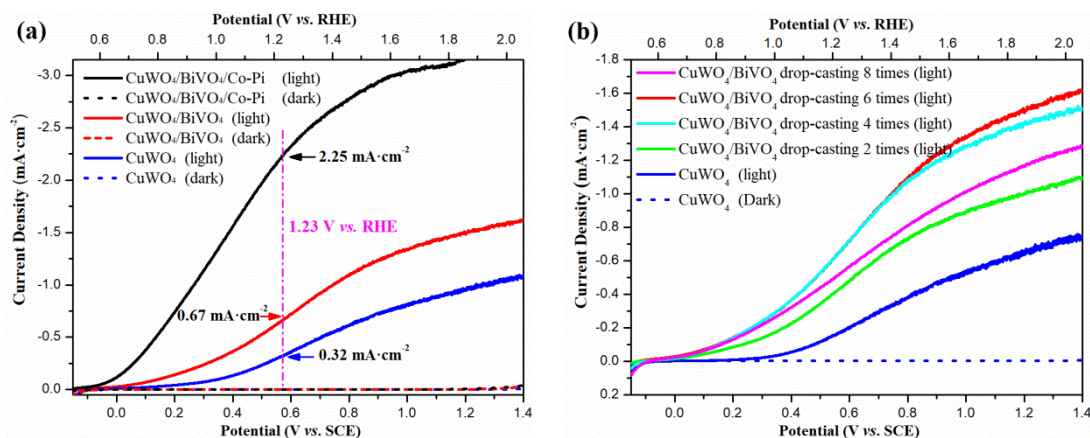
Figure 4. (**a**) Linear sweep voltammograms of the $CuWO_4$, $CuWO_4/BiVO_4$, and $CuWO_4/BiVO_4/Co$-Pi-composite photoanodes in 1.0 M of Na_2SO_4 with 0.1 M of sodium phosphate buffer (pH = 7) in the dark and under illumination (100 mW·cm^2); (**b**) Variation of the photocurrent density as a function of the drop-casting times of the Bi precursor solution on $CuWO_4$. The pure $CuWO_4$ sample in (**b**) experienced the same preparation procedure as the $CuWO_4/BiVO_4$ composite (drop-casting 6 times) except that no Bi precursor existed in the drop-casting solution.

We also investigated the influence of the deposition amount of $BiVO_4$ on $CuWO_4$, and the results are shown in Figure 4b. To elucidate the effect of the preparation procedure (drop-casting, drying and annealing) on the activity of $CuWO_4$, Figure 4b presents the LSV curves of pure $CuWO_4$ that experienced the same preparation steps as the $CuWO_4/BiVO_4$ composite (drop-casting 6 times) except that no Bi precursor (Bi $(NO_3)_3$) existed in the drop-casting solution. By comparing the photocurrent density of the pure $CuWO_4$ in Figure 4a,b, we found that the aforementioned preparation procedure decreased the activity of $CuWO_4$. However, the presence of $BiVO_4$ not only compensated for the negative effect of the preparation procedure on the activity of $CuWO_4$, but also led to a significantly improved photocurrent density on the resulting $CuWO_4/BiVO_4$ composite. This result provided further evidence that the formation of the $CuWO_4/BiVO_4$ heterojunction was crucial for the enhancement of the activity toward the PEC OER.

Figure 4b clearly demonstrates that, as the drop-casting times were increased, the photocurrent density of the $CuWO_4/BiVO_4$ composite first increased and then decreased, with the sample prepared by drop-casting 6 times exhibiting the highest activity. We believed that the thickness of the outer $BiVO_4$ layer was the key factor controlling the activity of the $CuWO_4/BiVO_4$ composite. As is self-evident, more drop-casting times inevitably resulted in thicker $BiVO_4$ layer, which improved the light absorption ability of the $BiVO_4$ layer but impaired the light absorption ability of the $CuWO_4$ layer. Therefore, there must be an optimal thickness of $BiVO_4$ that balances the two opposite effects.

We believe that the $CuWO_4/BiVO_4$ sample prepared by drop-casting 6 times had the optimal $BiVO_4$ thickness, and as a result, it exhibited the highest activity toward the PEC OER.

It has been reported that Co-Pi and cobalt borate (Co-Bi) could be well coupled with $BiVO_4$ as a co-catalyst, and J_{ph} on the resulting $BiVO_4$/Co-Pi (or Co-Bi) at 1.23 V versus RHE was increased to over 2.5–3 times the value on $BiVO_4$ [11,12]. This work inspired us to combine the $CuWO_4/BiVO_4$ composite with Co-Pi, as in our study, the $BiVO_4$ was the outermost layer that could be used to deposit Co-Pi. Figure 4a clearly shows that coupling $CuWO_4/BiVO_4$ with Co-Pi led to a significant improvement of J_{ph}, and the value of J_{ph} at 1.23 V versus RHE was 2.25 mA·cm^{-2}, which is among the highest reported on $CuWO_4$ [13–20] and $CuWO_4/BiVO_4$ photoanodes [14,24].

Figure 5 shows the schematic representation of the energy band structure of the $CuWO_4/BiVO_4$/Co-Pi composite and the corresponding charge transfer mechanism during illumination. We believe there were three main reasons for the high activity of the composite for the PER OER. First, the nano-network structure of the composite provided a large specific surface area that ensured a high probability of light–semiconductor interaction and a large composite/solution interface, both benefitting the improvement of the activity for the OER. Second, both the conduction and valence band edges of $BiVO_4$ are higher than those of $CuWO_4$, making a well-matched energy band structure for the $CuWO_4/BiVO_4$ heterojunction. The heterojunction led to a more efficient separation of the photoinduced electron–hole pairs, as the photoinduced holes were driven to the surface of $BiVO_4$ and the electrons were injected into $CuWO_4$ and then driven into FTO under applied potential. Third, the holes that moved to the surface of $BiVO_4$ could be captured by Co-Pi and resulted in the generation of a high valence state of the Co species, such as Co (IV) [26,27], which were highly active toward the oxidized water.
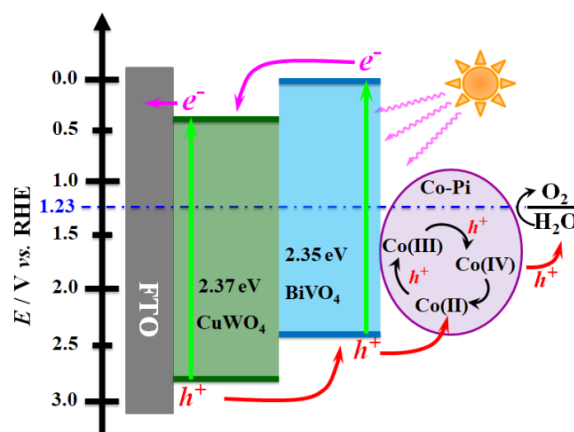
Figure 5. Schematic representation of the energy band structure of the $CuWO_4/BiVO_4$ heterojunction and charge transfer mechanism during illumination.

3. Materials and Methods

3.1. Materials

Cupric nitrate trihydrate ($Cu(NO)_3 \cdot 3H_2O$) was purchased from Sinopharm Chemical Reagent Co., Ltd. (Beijing, China). Tungsten powder, tungstic acid (H_2WO_4), hydrogen peroxide (H_2O_2), absolute ethyl alcohol, isopropanol, potassium hydroxide (KOH), urea, acetonitrile, oxalic acid, hydrochloric acid (HCl), and acetic acid ($C_2H_4O_2$) were purchased from Beijing Chemical Works (Beijing, China). All the chemicals were of analytical grade and used without further purification. All the aqueous solutions were prepared using deionized water (>18 MΩ). Fluorine-doped tin oxide (FTO) substrates (8 Ω·sq^{-1}, transparency 80%) were purchased from Asahi Glass, Tokyo, Japan.

3.2. Preparation of Network-Structured CuWO₄/BiVO₄ and CuWO₄/BiVO₄/Co-Pi Nanocomposites

The WO_3 NFs were first prepared on the FTO substrate via a nanoseed-assisted hydrothermal method [13], and then, they were used as sacrificial templates to synthesize $CuWO_4$ NFs via a thermal solid phase reaction between WO_3 NFs and CuO [13]. Then, the obtained $CuWO_4$ NFs were used as supports to synthesize the network-structured $CuWO_4/BiVO_4$ nanocomposite. In detail, Bi $(NO_3)_3 \cdot 5H_2O$ and vanadyl acetylacetonate were dissolved in a mixed solvent of glacial acetic acid and acetylacetone (20:1, volume ratio) to get a final concentration of 10 mM and 9.3 mM, respectively. Then, 20 µL of the mixed solution was drop-cast onto the FTO-supported $CuWO_4$ NFs, and the sample was put into a 400 °C oven for 2 min to dry the drop-casting solution. This step was repeated for the required times to modulate the amount of bismuth precursor. Then, the dried samples were annealed in air at 550 °C for 2 h to obtain the $CuWO_4/BiVO_4$ composite. Pure $BiVO_4$ films were also prepared using the same method in which the mixed precursor solution was drop-casted on bare FTO substrates. The Co-Pi layer was deposited onto the surface of $CuWO_4/BiVO_4$ using a photo-assisted electrodeposition method described in our previous work [6].

3.3. Characterization

The morphology of the WO_3, $CuWO_4$, and $CuWO_4/BiVO_4$-composite NFs were characterized by a Hitachi S-4800 field emission scanning electron microscope operating (Tokyo, Japan) at an accelerating voltage of 10 kV. High-resolution transmission electron microscopic images were obtained on a field emission JEM-2010F microscope (JEOL Ltd., Tokyo, Japan) with an accelerating voltage of 200 kV. The X-ray diffraction (XRD) pattern of the $CuWO_4$, $BiVO_4$, and $CuWO_4/BiVO_4$-composite NFs were collected by an X-ray diffractometer (Rigaku, rint2000 advance theta-2theta powder diffractometer, Tokyo, Japan) with Cu Kα radiation. UV–Vis diffuse reflection spectra were recorded on a UV–Vis-NIR spectrophotometer (Shimadzu 3600, Kyoto, Japan).

3.4. Photoelectrochemical Measurements

Photoelectrochemical measurements were conducted on a CHI660D workstation (CH Instruments Co., Austin, TX, USA), while a 300 W xenon lamp served as the light source. The light intensity illuminated on the surface of all the photoelectrodes was calibrated to 100 mW·cm^{-2}. All the electrochemical measurements were performed in a three-electrode photoelectrochemical cell in 1.0 M of Na_2SO_4 with 0.1 M of sodium phosphate buffer (pH = 7), and Pt and saturated calomel electrode (SCE) serving as counter and reference electrodes, respectively. All the potentials in this work were reported with reference to SCE and RHE.

4. Conclusions

In summary, we successfully prepared the $CuWO_4/BiVO_4$ film by using $CuWO_4$ NFs as templates via a simple method that combined drop-casting and thermal annealing. The obtained $CuWO_4/BiVO_4$ film had a network structure that was composed of intersected $CuWO_4/BiVO_4$-composite NFs. The $CuWO_4/BiVO_4$ showed significantly improve activity for PER OER as compared with $CuWO_4$. We further improved the activity by coupling co-catalyst Co-Pi with $CuWO_4/BiVO_4$. A photocurrent density of 2.25 mA·cm^{-2} was obtained on the $CuWO_4/BiVO_4/Co-Pi$ composite, and this value was among the highest reported on $CuWO_4$-based photoanodes in a neutral solution. The high activity for the PEC OER was attributed to the following three reasons: (1) The high specific surface area of the composite greatly increased the light absorption probability and the electrode/solution interface; (2) the $CuWO_4/BiVO_4$ heterojunction accelerated the separation of the photoinduced electron–hole pairs; and (3) the presence of the Co-Pi co-catalyst significantly improved the charge transfer across the composite/solution interface. Although $CuWO_4$ is still no match for the highly efficient photoanode materials right now, this work demonstrates both the potential of $CuWO_4$ as a photoanode for OER and the strategy to improve its performance.

References

1. Gratzel, M. Photoelectrochemical cells. *Nature* **2001**, *414*, 338–344. [CrossRef] [PubMed]
2. Fujishima, A.; Honda, K. Electrochemical Photolysis of Water at a Semiconductor Electrode. *Nature* **1972**, *238*, 37–38. [CrossRef] [PubMed]
3. Steinmiller, E.M.P.; Choi, K.-S. Photochemical deposition of cobalt-based oxygen evolving catalyst on a semiconductor photoanode for solar oxygen production. *Proc. Natl. Acad. Sci. USA* **2009**, *106*, 20633–20636. [CrossRef] [PubMed]
4. Mishra, Y.K.; Adelung, R. ZnO tetrapod materials for functional applications. *Mater. Today* **2018**, *21*, 631–651. [CrossRef]
5. Jin, T.; Diao, P.; Xu, D.; Wu, Q. High-aspect-ratio WO_3 nanoneedles modified with nickel-borate for efficient photoelectrochemical water oxidation. *Electrochim. Acta* **2013**, *114*, 271–277. [CrossRef]
6. Jin, T.; Diao, P.; Wu, Q.; Xu, D.; Hu, D.; Xie, Y.; Zhang, M. WO_3 nanoneedles/α-Fe_2O_3/cobalt phosphate composite photoanode for efficient photoelectrochemical water splitting. *Appl. Catal. B Environ.* **2014**, *148–149*, 304–310. [CrossRef]
7. Hu, D.; Diao, P.; Xu, D.; Wu, Q. Gold/WO_3 nanocomposite photoanodes for plasmonic solar water splitting. *Nano Res.* **2016**, *9*, 1735–1751. [CrossRef]
8. Jin, T.; Xu, D.; Diao, P.; He, W.-p.; Wang, H.-w.; Liao, S.-z. Tailored preparation of WO_3 nano-grassblades on FTO substrate for photoelectrochemical water splitting. *CrystEngComm* **2016**, *18*, 6798–6808. [CrossRef]
9. Wu, Q.; Xu, D.; Xue, N.; Liu, T.; Xiang, M.; Diao, P. Photo-catalyzed surface hydrolysis of iridium(iii) ions on semiconductors: A facile method for the preparation of semiconductor/IrOx composite photoanodes toward oxygen evolution reaction. *Phys. Chem. Chem. Phys.* **2017**, *19*, 145–154. [CrossRef] [PubMed]
10. Wu, Q.; Diao, P.; Sun, J.; Xu, D.; Jin, T.; Xiang, M. Draining the photoinduced electrons away from an anode: The preparation of Ag/Ag_3PO_4 composite nanoplate photoanodes for highly efficient water splitting. *J. Mater. Chem. A* **2015**, *3*, 18991–18999. [CrossRef]
11. Ding, C.; Shi, J.; Wang, D.; Wang, Z.; Wang, N.; Liu, G.; Xiong, F.; Li, C. Visible light driven overall water splitting using cocatalyst/$BiVO_4$ photoanode with minimized bias. *Phys. Chem. Chem. Phys.* **2013**, *15*, 4589–4595. [CrossRef] [PubMed]
12. Abdi, F.F.; van de Krol, R. Nature and Light Dependence of Bulk Recombination in Co-Pi-Catalyzed $BiVO_4$ Photoanodes. *J. Phys. Chem. C* **2012**, *116*, 9398–9404. [CrossRef]
13. Hu, D.; Diao, P.; Xu, D.; Xia, M.; Gu, Y.; Wu, Q.; Li, C.; Yang, S. Copper(ii) tungstate nanoflake array films: Sacrificial template synthesis, hydrogen treatment, and their application as photoanodes in solar water splitting. *Nanoscale* **2016**, *8*, 5892–5901. [CrossRef] [PubMed]
14. Ye, W.; Chen, F.; Zhao, F.; Han, N.; Li, Y. $CuWO_4$ Nanoflake Array-Based Single-Junction and Heterojunction Photoanodes for Photoelectrochemical Water Oxidation. *ACS Appl. Mater. Interfaces* **2016**, *8*, 9211–9217. [CrossRef] [PubMed]
15. Hill, J.C.; Choi, K.-S. Synthesis and characterization of high surface area $CuWO_4$ and Bi_2WO_6 electrodes for use as photoanodes for solar water oxidation. *J. Mater. Chem. A* **2013**, *1*, 5006–5014. [CrossRef]
16. Pyper, K.J.; Yourey, J.E.; Bartlett, B.M. Reactivity of $CuWO_4$ in Photoelectrochemical Water Oxidation Is Dictated by a Midgap Electronic State. *J. Phys. Chem. C* **2013**, *117*, 24726–24732. [CrossRef]
17. Yourey, J.E.; Bartlett, B.M. Electrochemical deposition and photoelectrochemistry of $CuWO_4$, a promising photoanode for water oxidation. *J. Mater. Chem.* **2011**, *21*, 7651–7660. [CrossRef]
18. Yourey, J.E.; Pyper, K.J.; Kurtz, J.B.; Bartlett, B.M. Chemical Stability of $CuWO_4$ for Photoelectrochemical Water Oxidation. *J. Phys. Chem. C* **2013**, *117*, 8708–8718. [CrossRef]

19. Zhou, M.; Liu, Z.; Li, X.; Liu, Z. Promising Three-Dimensional Flowerlike $CuWO_4$ Photoanode Modified with CdS and FeOOH for Efficient Photoelectrochemical Water Splitting. *Ind. Eng. Chem. Res.* **2018**, *57*, 6210–6217. [CrossRef]

20. Nam, K.M.; Cheon, E.A.; Shin, W.J.; Bard, A.J. Improved Photoelectrochemical Water Oxidation by the $WO_3/CuWO_4$ Composite with a Manganese Phosphate Electrocatalyst. *Langmuir* **2015**, *31*, 10897–10903. [CrossRef] [PubMed]

21. Hong, S.J.; Lee, S.; Jang, J.S.; Lee, J.S. Heterojunction $BiVO_4/WO_3$ electrodes for enhanced photoactivity of water oxidation. *Energy Environ. Sci.* **2011**, *4*, 1781–1787. [CrossRef]

22. Su, J.; Guo, L.; Bao, N.; Grimes, C.A. Nanostructured $WO_3/BiVO_4$ Heterojunction Films for Efficient Photoelectrochemical Water Splitting. *Nano Lett.* **2011**, *11*, 1928–1933. [CrossRef] [PubMed]

23. Xia, L.; Bai, J.; Li, J.; Zeng, Q.; Li, L.; Zhou, B. High-performance $BiVO_4$ photoanodes cocatalyzed with an ultrathin α-Fe_2O_3 layer for photoelectrochemical application. *Appl. Catal. B Environ.* **2017**, *204*, 127–133. [CrossRef]

24. Pilli, S.K.; Deutsch, T.G.; Furtak, T.E.; Brown, L.D.; Turner, J.A.; Herring, A.M. $BiVO_{(4)}/CuWO_{(4)}$ heterojunction photoanodes for efficient solar driven water oxidation. *Phys. Chem. Chem. Phys.* **2013**, *15*, 3273–3278. [CrossRef] [PubMed]

25. Zheng, F.; Guo, M.; Zhang, M. Hydrothermal preparation and optical properties of orientation-controlled WO_3 nanorod arrays on ITO substrates. *CrystEngComm* **2013**, *15*, 277–284. [CrossRef]

26. Kanan, M.W.; Yano, J.; Surendranath, Y.; Dincă, M.; Yachandra, V.K.; Nocera, D.G. Structure and Valency of a Cobalt−Phosphate Water Oxidation Catalyst Determined by in Situ X-ray Spectroscopy. *J. Am. Chem. Soc.* **2010**, *132*, 13692–13701. [CrossRef] [PubMed]

27. Symes, M.D.; Surendranath, Y.; Lutterman, D.A.; Nocera, D.G. Bidirectional and Unidirectional PCET in a Molecular Model of a Cobalt-Based Oxygen-Evolving Catalyst. *J. Am. Chem. Soc.* **2011**, *133*, 5174–5177. [CrossRef] [PubMed]